Computational simulations integrating inhibition kinetics of tyrosinase by oxalic acid

Li Yan[1], Shang-Jun Yin[2], Daeui Park[3], Yue-Xiu Si[2], Zhi-Jiang Wang[2], Hae Young Chung[3], Jun-Mo Yang[4], *Guo-Ying Qian[2], *Yong-Doo Park[1,2]

[1]Zhejiang Provincial Key Laboratory of Applied Enzymology, Yangtze Delta Region Institute of Tsinghua University, Jiaxing 314006, P. R. China.
[2]College of Biological and Environmental Sciences, Zhejiang Wanli University, Ningbo 315100, P. R. China.
[3]Molecular Inflammation Research Center for Aging Intervention (MRCA), College of Pharmacy, Pusan National University, Busan 609-735, Korea.
[4]Department of Dermatology, Sungkyunkwan University School of Medicine, Samsung Medical Center, Seoul 135-710, Korea.

Tyrosinase inhibition studies are important for agricultural and medicinal applications. Computational predictions and enzymatic assays via kinetics may be used to detect effective inhibitors of tyrosinase. We predicted the 3D structure of tyrosinase from *Agaricus bisporus*, used a docking algorithm to simulate binding between tyrosinase and oxalic acid (OA), and studied the reversible inhibition of tyrosinase by OA. Simulations were successful (binding energies for Dock6.3 = -18.76 and AutoDock4.2 = -2.47 kcal/mol), suggesting that OA interacts with the LYS224 residue that is predicted by both programs. OA inhibited tyrosinase in a mixed-type manner with a K_i = 3.16 ± 1.8 mM and IC_{50} = 8.0 ± 0.5 mM. Measurements of intrinsic and ANS-binding fluorescences showed that OA induced changes in the active site structure. Our results suggest that the strategy of predicting tyrosinase inhibition based on carboxyl groups and orientation may prove useful for the screening of potential tyrosinase inhibitors.

Key Words: Tyrosinase, oxalic acid, docking simulation, inhibition kinetics, mixed-type, carboxyl group

INTRODUCTION

Tyrosinase (EC 1.14.18.1) is a ubiquitous enzyme with diverse physiologic roles related to pigment production. Tyrosinase plays a central role in melanin synthesis in the skin (Jimbow et al., 2000; Olivares and Solano, 2009), the browning of vegetables (Rescigno et al., 2002; Kim and Uyama, 2005), wound healing (Lai et al., 2002; Kanost et al., 2004), and cuticle formation in insects (Guerrero and Rosell, 2005). Therefore, tyrosinase inhibitors have potential applications in medicine and cosmetics as whitening agents, and in agriculture as bio-insecticides. With respect to catalysis, tyrosinase belongs to the type 3 copper protein family (Li et al., 2009; Yoon et al., 2009), with two copper ions that are each coordinately bonded with a distinct set of three histidine residues within the active site. These coppers participate directly in the hydroxylation of monophenols to *o*-diphenols (cresolase activity) and in the oxidation of *o*-diphenols to *o*-quinones (catechol oxidase activity) (Decker and Tuczek, 2000). The tyrosinase mechanism is complex, and this enzyme can catalyze multiple reactions. The overall 3D structure and architecture of the active site are not well understood. Thus, studies of this enzyme

List of Abbreviations

OA, oxalic acid; DOPA, 3,4-dihydroxyphenylalanine; ANS, 1-anilinonaphthalene-8-sulfonate

mechanism must involve a variety of computational methods and kinetics to derive the structure-function relationships, e.g., between substrates and ligands of the enzyme.

In the current study we determined the mechanism of tyrosinase inhibition by oxalic acid (OA) using computational simulation and kinetic analysis. We hypothesized that the two dicarboxylic acids of OA may block L-DOPA oxidation by binding to tyrosinase. Previous findings have shown the importance of carboxyl groups in tyrosinase inhibition (Yokota et al., 1998; Shiino et al., 2001, 2003; Kim et al., 2006; Kanade et al., 2007; Yan et al., 2009; Yamazaki et al., 2009) in terms of molecular position, number, and specific interactions with the enzyme; these findings further support our hypothesis. OA has two carboxyl groups, thus implying that OA might have an inhibitory effect on tyrosinase. OA is present in many organisms (Gadd, 1999; Zoppi et al., 2010; Lehner et al., 2008; Zou et al., 2007). The spinach family contains high levels of OA (Betsche and Fretzdorff, 2005; genannt Bonsmann et al., 2008). Some bacteria also produce oxalates from the oxidation of carbohydrates (Nakata and He, 2010). Regardless of its occurrence in nature and potential use as a food additive (Sayyari et al., 2010; Gao et al., 2010; Anang et al., 2006), the direct use of OA in medicinal or cosmetic applications is limited due to its toxicity. However, effective approaches derived from the combination of computational simulation and enzymatic kinetics are of interest for further screening of tyrosinase inhibitor candidates. The results of computational simulation suggest that OA could be a potent inhibitor of tyrosinase, because OA directly interacts with some residues that are located near the active site. Experimentally, OA exerts mixed-type inhibition on tyrosinase. Kinetic parameters consistently support the results of docking simulations, and measurements of ANS-binding fluorescence reveal changes in regional structure. A combination of inhibition kinetics and computational modeling may facilitate the testing of potential tyrosinase inhibitors, such as OA and predictions of the inhibitory mechanisms that are involved.

MATERIALS AND METHODS

Materials

Tyrosinase (M.W. 128 kDa), L-DOPA, and OA were purchased from Sigma-Aldrich (Seoul, Korea). When L-DOPA was used as a substrate in our experiments, the purchased tyrosinase had a K_m of 0.22 ± 0.15 mM (V_{max} = 0.14 ± 0.02 mmol·min^{-1}) according to a Lineweaver-Burk plot.

Tyrosinase assay

A spectrophotometric tyrosinase assay was performed as previously described (Park et al., 2005; Han et al., 2007). To begin the assay, a 10-µl sample of enzyme solution was added to 1 ml of reaction mix. Tyrosinase activity (v) was recorded as the change in absorbance per min at 492 nm using a Perkin Elmer Lambda Bio U/V spectrophotometer.

Homology modeling of tyrosinase

The 3D structure of tyrosinase from *Agaricus bisporus* was modeled using the SWISS-MODEL (Arnold et al., 2006) to assemble 556 amino acids (Protein CAA11562) that were selected using a homology-modeling protocol. This method differs from those described in previous reports (Gou et al., 2008; Lü et al., 2010). We retrieved the known homologues of tyrosinase (average, 23% sequence identity), as well as partial tyrosinase homologues, from the Protein Data Bank (PDB) (http://www.pdb.org) and identified a PDB entry (2zmx chain A) to provide a suitable structural template. Based on the sequence alignment, the 3D structure of tyrosinase was constructed with a high level of confidence (final total energy, 38297.020 KJ/mol).

Molecular docking of tyrosinase and OA

Among the many tools available for protein-ligand docking, Autodock4.2 and Dock6.3 programs were applied because of their automated capabilities (Morris et al., 2009). The programs use a set of predefined 3D grids of the target protein with a systematic search technique (Huey et al., 2007). The original structure of OA was derived from the PubChem database (Compound ID: 7489, http://pubchem.ncbi.nlm.nih.gov/). To prepare for the docking procedure, the following steps were taken, 1 conversion of 2D structures to 3D structures, 2 calculation of charges, 3 addition of hydrogen atoms, 4 location of pockets. For these steps, we used Open Eye (http://www.eyesopen.com).

Kinetic analysis of mixed-type inhibition

To describe the mixed-type inhibition mechanism, the Lineweaver-Burk equation in double reciprocal form can be written as:

$$\frac{1}{v} = \frac{K_m}{V_{max}}\left(1+\frac{[I]}{K_i}\right)\frac{1}{[S]} + \frac{1}{V_{max}}\left(1+\frac{[I]}{\alpha K_i}\right) \qquad (1)$$

Secondary plots can be constructed from

$$Slope = \frac{K_m}{V_{max}} + \frac{K_m[\mathrm{I}]}{V_{max}K_i} \quad (2)$$

and *Y-intercept*

$$= \frac{1}{V_{max}^{app}} = \frac{1}{V_{max}} + \frac{1}{\alpha K_i V_{max}}[\mathrm{I}] \quad (3)$$

Then, the *α*, K_i, K_m, and V_{max} values can be derived from the above equations. The secondary replot of *Slope* or *Y-intercept* vs. [I] is linearly-fitted, assuming a single inhibition site or a single class of inhibition site, as shown: Scheme1.

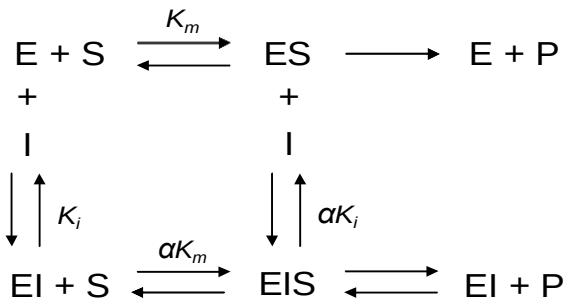

Scheme 1. E, enzyme tyrosinase; S, substrate L-DOPA; I, inhibitor OA; P, product DOPAchrome; K_i, inhibitor dissociation constant; α, modifying factor.
The OA binds to the E and ES complex.

Intrinsic and ANS-binding fluorescence measurements

Fluorescence emission spectra were measured with a Jasco FP750 spectrofluorometer using a cuvette with a 1-cm path length. Tryptophan fluorescence was measured following excitation at 280 nm, and the emission wavelength ranged between 300 and 410 nm. Changes in the ANS-binding fluorescence of tyrosinase were measured following excitation at 390 nm, and the emission wavelength ranged from 400-520 nm. The tyrosinase was labeled with 40 µM ANS for 30 min prior to measurements.

All kinetic reactions and measurements in this study were performed in 50 mM sodium phosphate buffer (pH 6.9).

Determination of the binding constant and the number of binding sites

According to a previous report (Xie et al., 2005), in which small molecules were bound to equivalent sites on a macromolecule, the equilibrium between free and bound molecules is given by the following equation:

$$\frac{F_0}{F_0 - F} = \frac{1}{n} + \frac{1}{K}\frac{1}{[Q]} \quad (4)$$

where F_0 and F are the relative steady-state fluorescence intensities in the absence and presence of quencher, respectively, and [*Q*] is the quencher (OA) concentration. The values of the binding constant (*K*) and number of binding sites (*n*) can be derived from the intercept and slope of a plot based on Equation. (4).

RESULTS

Computational prediction of 3D tyrosinase structure and docking simulation of OA binding

Because the crystallographic structure of tyrosinase is not available, we selected a template structure from the PDB (2zmxA) to simulate the 3D structure of tyrosinase (Figure. 1). In the predicted structure of tyrosinase, a binding pocket is indicated with two coppers: one is coordinated to HIS38, HIS54, and HIS63 and the other is coordinated to HIS190, HIS194, and HIS216, respectively. The docking simulation of binding between OA and tyrosinase was successful in producing a significant score (the binding energy for Dock6.3 was -18.76 kcal/mol). We searched for OA-binding residues within tyrosinase that were close to each other and found the most important residues at LYS66, GLU67, PRO69, LYS75, ALA76, LYS224, and ASN226 predicted by Dock6.3.

In the same manner, AutoDock4.2 was also applied to probe docking sites (Figure. 2). As a result, OA-binding residues with significant scores were predicted as LYS224, PRO315, and ASN316 (binding energy for AutoDock4.2 was -2.47 kcal/mol). We found that LYS224 was commonly predicted by both programs. The docking simulations provided data indicating that OA is a tyrosinase inhibitor candidate by identifying binding residues near the active site pocket that might directly affect the L-DOPA substrate docking and catalysis.

Effect of OA on tyrosinase activity: inhibition kinetics

In the next step, we assayed changes in tyrosinase activity in the presence of OA to confirm the results of docking simulations. Tyrosinase activity was conspicuously inactivated by OA in a dose-dependent manner with an IC_{50} of 8.0 ± 0.5 mM (*n* = 2) when OA was present both in reaction and assay buffers (Figure. 3A). At less than 100 mM OA, tyrosinase was completely inactive (Figure. 3A). When OA was removed from the

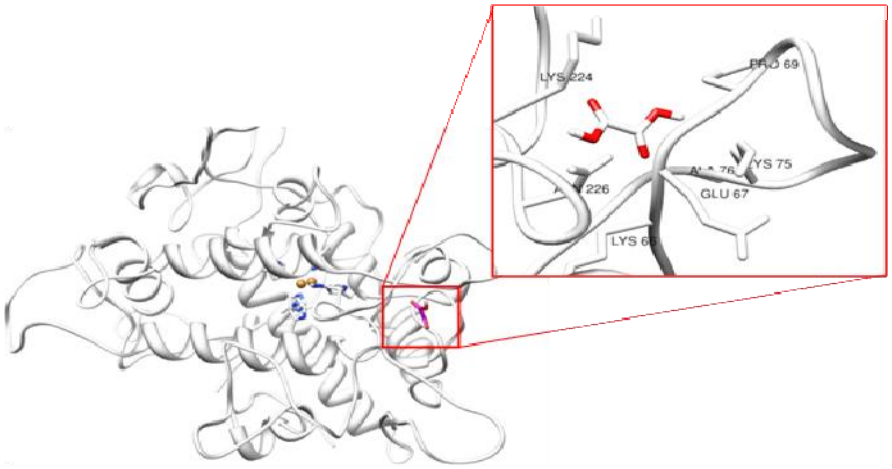

Figure 1. Computational docking simulation by Dock6.3 between tyrosinase and OA . Sequence alignment between tyrosinase (Protein CAA11562) and the selected PDB entry (2zmx chain A: average of 23% sequence identity) was conducted to provide a suitable structural template. The 3D structure of tyrosinase was constructed using SWISS-MODEL to assemble 556 amino acids that were selected through a homology-modeling protocol. Two copper ions (balls) were coordinated with six histidines, as indicated. The red stick represents OA as docked by Dock6.3.

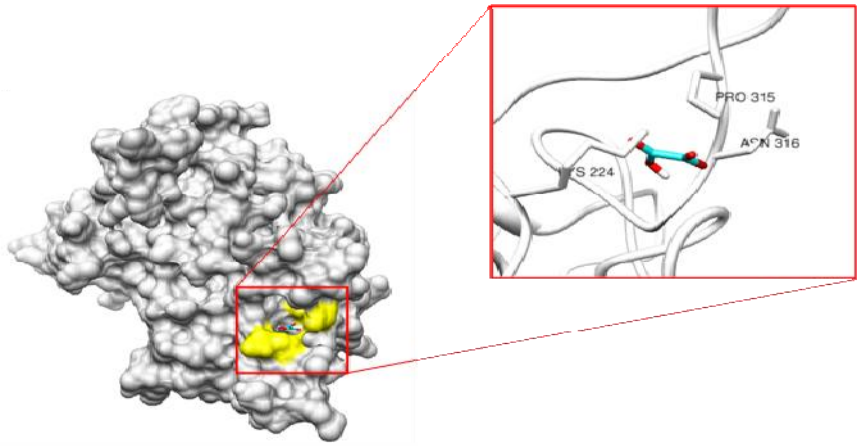

Figure 2. Computational docking simulation by AutoDock4.2 between tyrosinase and OA. The yellow zone indicates the location of the binding site, and the red boxes indicate putative OA-binding sites. The stick is OA as docked by AutoDock4.2.

assay buffer, the value of IC_{50} was shifted to 22.5 ± 3.54 mM (n = 2), showing that OA reversibly binds to tyrosinase (Figure. 3B).

To confirm the reversibility of OA-mediated inhibition, plots of the remaining activity versus [E] were constructed (Figure. 4). The results showed straight lines passing through the origin, indicating OA-mediated reversible inhibition, as predicted in the results of Figure. 3.

Lineweaver-Burk plot analysis of tyrosinase inhibition by OA

We adapted Lineweaver-Burk plot analysis to elucidate the inhibition type of OA on tyrosinase. The results showed changes in both apparent V_{max} and K_m, indicating that OA induced a mixed-type of inhibition (Figure. 5A). The secondary replot of *Slope* vs. [OA] was linearly-fitted

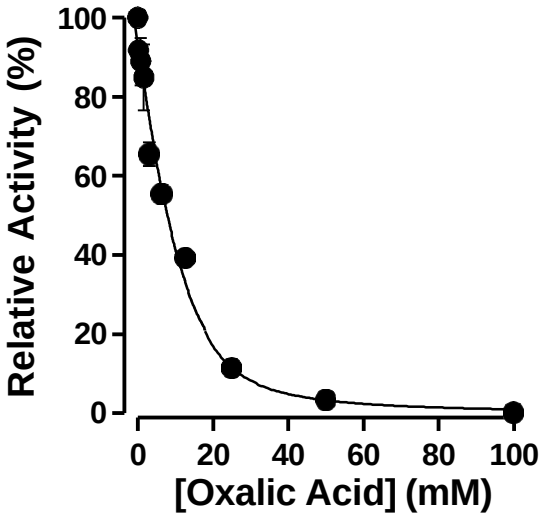

Figure 3 (A). Inhibitory effect of OA on tyrosinase.

Data are presented as means (*n* = 3). Tyrosinase was incubated with OA at various concentrations for 3 h at 25 ºC and then added to the assay system at the corresponding OA concentrations (A) or in the absence of OA

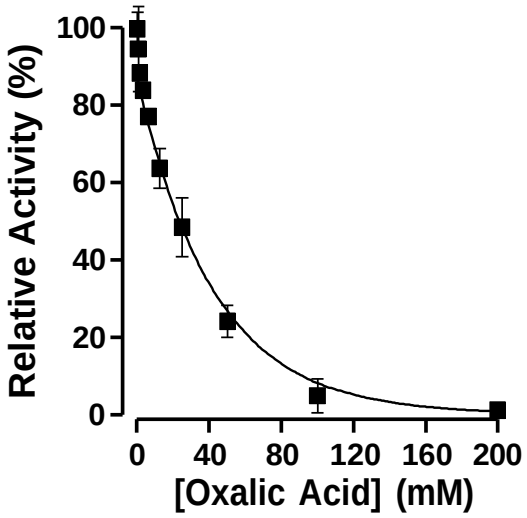

Figure 3 (B). The final concentrations of L-DOPA and tyrosinase were 2 mM and 2.0 µg/ml, respectively.

(Figure. 5B), showing that OA has a single inhibition site or a single class of inhibition site on tyrosinase. Using Equations. (1)-(3), the ɑ-value was calculated to be 3.60 ± 1.0 (*n* = 2) and the K_i was 3.16 ± 1.8 mM (*n* = 2). V_{max} value changes predicted by docking simulations indicated that OA might not compete with L-DOPA for docking, because the binding sites are not located in the active site pocket. However, the K_m changes occurred in a more complex manner: L-DOPA does not directly compete with OA but the L-DOPA accessibility for docking to coppers at the active site could be affected by OA-docking induced conformational changes that produce the tertiary shape

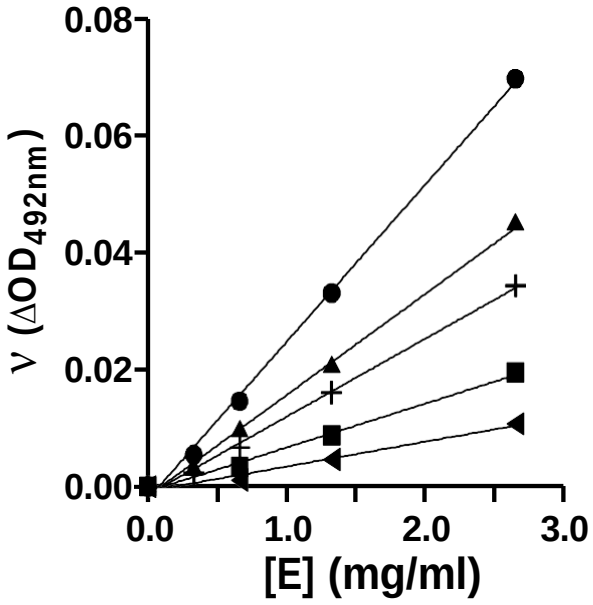

Figure 4. Plots of *v* versus [E].
The *v* value indicates the change in absorbance at 492 nm per min at OA concentrations of 0 (●), 12.5 (▲), 25 (+), 50 (■), and 75 (◄) mM. The final L-DOPA concentration was 2 mM.

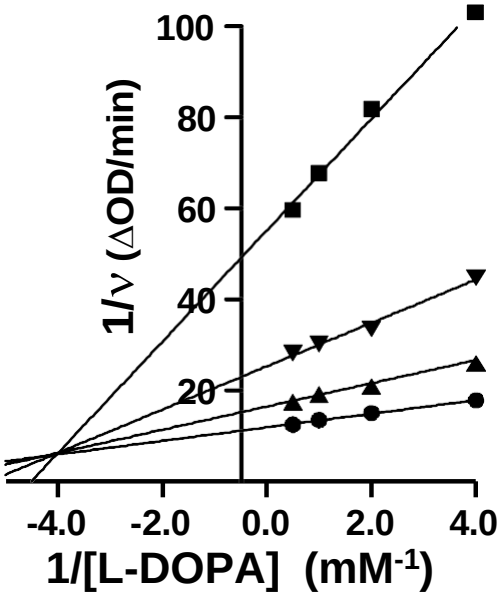

Figure 5. Lineweaver-Burk plots.
(A) The OA concentrations were 0 (●), 12.5 (▲), 25 (▼), and 50 mM (■). The final enzyme concentration was 2.0 µg/ml.

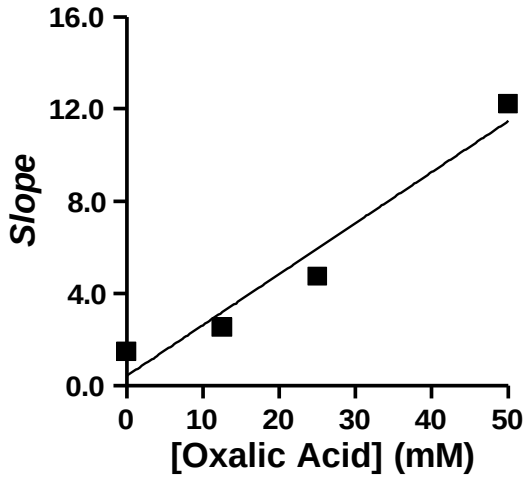

Figure 5 (B) Secondary replot of *Slope* vs. [OA]. All data were collected from Lineweaver-Burk plots. The replots were plotted based on Eq. (2).

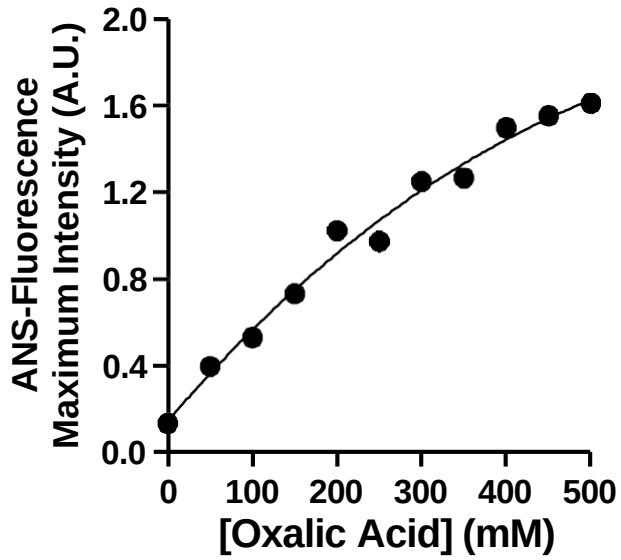

Figure 6. Changes in ANS-binding fluorescence of tyrosinase at different OA concentrations.
ANS (40 µM) was incubated with tyrosinase for 30 min to label hydrophobic enzyme surfaces prior to fluorescence measurements. Data are presented as means (*n* = 2).

of the active site. These conformational changes might be monitored by hydrophobic surface changes of tyrosinase because the OA docking site is very near the active site where L-DOPA oxidation occurs. Thus, mixed-type inhibition of tyrosinase by OA was observed. Overall, the experimental data agreed well with the predictions of equations and simulations.

Effect of OA on tyrosinase tertiary structure: spectrofluorimetry studies

Next, to confirm our hypothesis that changes in tyrosinase hydrophobicity occur due to alterations of the active site shape by OA, ANS-binding fluorescence changes were monitored in the presence of OA (Figure.6).

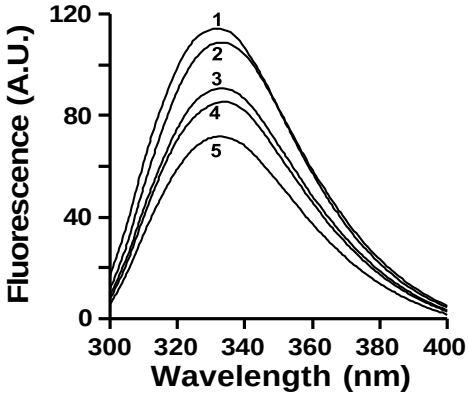

Figure 7 (A). Changes in intrintsic tyrosinase fluorescence at different OA concentrations. (A) Intrinsic fluorescence changes at high concentrations of OA. Tyrosinase was incubated with OA for 3 h before measurements. Label 1 represents the native state. Labels 2 through 5 indicate OA concentrations of 0.2, 0.3, 0.4, and 0.5 M, respectively.

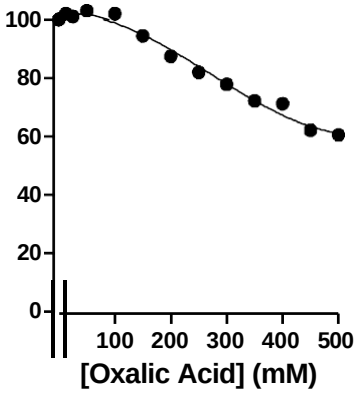

Figure 7(B) Plot of maximum fluorescence intensity vs. [OA]. Tyrosinase was incubated with various concentrations of OA (12.5 to 500 mM)

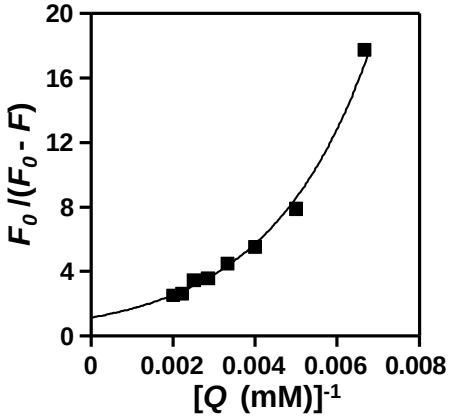

Figure 7 (C) Double reciprocal plot of $F_0/(F_0-F)$ vs. $[Q]^{-1}$. Equation [4] in Materials and Methods was applied. F_0, maximum native fluorescence intensity; F, maximum fluorescence intensity of sample; Q, quencher OA.

OA gradually altered the ANS-binding fluorescence of tyrosinase in a dose-dependent manner, an indication that binding to inhibitor exposed hydrophobic surfaces within tyrosinase, perhaps primarily due to the active site.

To compare this result further, we measured the intrinsic fluorescence changes of tyrosinase in the presence of OA. We found that the intrinsic fluorescence of tyrosinase changes significantly at higher than 100 mM OA accompanying a quenching effect, which gradually decreased with no significant shift of the maximum peak wavelength (Figure. 7A). However, at less than 100 mM, OA did not modulate the fluorescence (Figure. 7B). This result indicated that OA did not induce conspicuous overall tertiary structural changes of tyrosinase at less than 100 mM. Interestingly, at this OA concentration range, the activity was completely abolished (Figure. 3) and hydrophobic changes are clearly observed (Figure. 6). These data support the hypothesis that hydrophobic exposure is caused mainly by the active site, and thus, L-DOPA accessibility for docking copper ions was influenced by OA-induced regional changes of active site shape resulting in K_m changes. If the OA-induced changes do not originate from the active site, but directly occur on its docking site, the overall intrinsic fluorescence changes might be conspicuous at less than 100 mM OA; otherwise, they mainly originate from the active site, which is monitored by hydrophobicity.

To calculate binding affinity, a double reciprocal plot was evaluated according to Equation. (4) as shown in Figure. 7C. The results did not reveal a linear relationship. We calculated the binding constant to be $K = 0.16 \pm 0.02$ mM^{-1} and the binding number to be $n = 1.02 \pm 0.12$ using Equation. (5). Thus, OA showed relatively strong binding affinity for tyrosinase in the absence of substrate, and one possible binding site was observed when L-DOPA was not associated with the reaction.

DISCUSSION

Previous studies have recognized an apparently potent inhibitory effect of compounds with carboxyl groups on tyrosinase (Yokota et al., 1998; Shiino et al., 2001, 2003; Kim et al., 2006; Kanade et al., 2007; Yan et al., 2009; Yamazaki et al., 2009). In this context, we hypothesized that OA could be a potent tyrosinase inhibitor due to its structure, which includes two carboxyl groups. To confirm our hypothesis, we simulated the docking between OA and tyrosinase and conducted kinetic studies. As a result, we found that OA was directly involved in tyrosinase inhibition not simply via copper chelation, but in a mixed-type manner. The inhibitory mechanism of OA was similar to those of copper chelators, but OA did not directly bind to coppers at the active site (Park et al., 2006a,b). OA induced inhibition in a complex manner by binding to the region near the active site, which directly induced changes in the active site structure. Using computational simulations, we predicted that OA that was bound directly to several residues (the most significant being LYS224) of tyrosinase. These residues are thought to be involved in the first stage of OA binding. Although the OA binding site is quite different from the L-DOPA binding site, it does not overlap with the L-DOPA binding site. However it is in relatively close proximity to the L-DOPA binding site, which may allow OA binding to interact with the enzyme-substrate intermediate or another step in catalysis (V_{max} changes). This interaction may induce detectable hydrophobic changes in the active site that may in turn retard L-DOPA accession (K_m changes).

The principal findings of our study include the following: i) OA binding to tyrosinase causes a mixed-type of inhibition; ii) OA inhibition of tyrosinase does not involve gross changes in tertiary structure at lower than 100 mM, but hydrophobic exposure occurs; iii) putative OA-binding residues were successfully predicted using a computational simulation (docking) located near the active site pocket; and iv) further studies of OA containing carboxyl groups as tyrosinase inhibitors may lead to the development of a new strategy for screening effective tyrosinase inhibitors.

Taken together, our study provides new insights into the roles of active site residues in tyrosinase catalysis and provides useful information regarding the 3D structure of tyrosinase. A combination of inhibition kinetics and computational modeling may facilitate the testing of potential tyrosinase inhibitors, such as OA, and the prediction of their inhibitory mechanisms. The present study also suggests that the strategy of predicting tyrosinase inhibition based on carboxyl groups and orientation may prove useful for the screening of potential tyrosinase inhibitors.

ACKNOWLEDGEMENTS

This work was supported by grants of Key Science and Technology Innovation Teams of Zhejiang Province (Grants No. 2009R50031 and No. 2009R50031-1) from the Science and Technology Department of Zhejiang Province. Dr. Hae Young Chung was supported by National Research Foundation of Korea (NRF) grant funded by the Korea government (MOST) (No. 20090083538) and would like to thank the Aging Tissue Bank for providing data. Dr. Jun-Mo Yang was supported by a grant (Grant No. C-A9-220-1) from Samsung Biomedical Research Institute. Dr. Guo-Ying Qian was supported by the Zhejiang Provincial Top Key Discipline of Modern Microbiology and Application (Grants No. KF2010006 and No. KF2010007). Dr. Yong-Doo Park was supported by a grant from the project of Zhejiang

Provincial Natural Science Foundation of China (Grant No. Y2091212).

REFERENCES

Anang DM, Rusul G, Radu S, Bakar J, Beuchat LR (2006). Inhibitory effect of oxalic acid on bacterial spoilage of raw chilled chicken. J. Food Prot. 69:1913-1919.

Arnold K, Bordoli L, Kopp J, Schwede T (2006). The SWISS-MODEL workspace: a web-based environment for protein structure homology modeling. Bioinformatics 22: 195-201.

Betsche T, Fretzdorff B (2005). Biodegradation of oxalic acid from spinach using cereal radicles. J. Agric. Food Chem. 53: 9751-9758.

Decker H, Tuczek F (2000). Tyrosinase/catecholoxidase activity of hemocyanins: structural basis and molecular mechanism. Trends Biochem. Sci. 25:392-397.

Gadd GM (1999). Fungal production of citric and oxalic acid: importance in metal speciation, physiology and biogeochemical processes. Adv. Microb. Physiol. 41:47-92.

Gao HY, Yaylayan VA, Yeboah F (2010). Oxalic acid-induced modifications of postglycation activity of lysozyme and its glycoforms. J. Agric. Food Chem. 58:6219-6225.

Genannt BSS, Walczyk T, Renggli S, Hurrell RF (2008). Oxalic acid does not influence nonhaem iron absorption in humans: a comparison of kale and spinach meals. Eur. J. Clin. Nutr. 62:336-341.

Gou L, Lü ZR, Park D, Oh SH, Shi L, Park SJ, Bhak, J, Park YD, Ren ZL, Zou F (2008). The effect of histidine residue modification on tyrosinase activity and conformation: inhibition kinetics and computational prediction. J. Biomol. Struct. Dyn. 26:395-402.

Guerrero A, Rosell G. (2005). Biorational approaches for insect control by enzymatic inhibition. Curr. Med. Chem. 12:461-469.

Han HY, Lee JR, Xu WA, Hahn MJ, Yang JM, Park YD (2007). Effect of Cl^- on tyrosinase: complex inhibition kinetics and biochemical implication. J. Biomol. Struct. Dyn. 25:165-171.

Huey R, Morris GM, Olson AJ, Goodsell DS (2007). A semiempirical free energy force field with charge-based desolvation. J. Comput. Chem. 28:1145-1152.

Jimbow K, Park JS, Kato F, Hirosaki K, Toyofuku K, Hua C, Yamashita T (2000). Assembly, target-signaling and intracellular transport of tyrosinase gene family proteins in the initial stage of melanosome biogenesis. Pigment Cell Res. 13:222-229.

Kanade SR, Suhas VL, Chandra N, Gowda LR (2007). Functional interaction of diphenols with polyphenol oxidase. Molecular determinants of substrate/inhibitor specificity. FEBS J. 274:4177-4187.

Kanost MR, Jiang H, Yu XQ (2004). Innate immune responses of a lepidopteran insect, Manduca sexta. Immunol. Rev. 198:97-105.

Kim YJ, Uyama H (2005). Tyrosinase inhibitors from natural and synthetic sources: structure, inhibition mechanism and perspective for the future. Cell Mol. Life Sci. 62: 1707-1723.

Kim D, Park J, Kim J, Han C, Yoon J, Kim N, Seo J, Lee C (2006). Flavonoids as mushroom tyrosinase inhibitors: a fluorescence quenching study. J. Agric. Food Chem. 54:935-941.

Lai SC, Chen CC, Hou RF (2002). Immunolocalization of prophenoloxidase in the process of wound healing in the mosquito Armigeres subalbatus (Diptera: Culicidae). J. Med. Entomol. 39:266-274.

Lehner A, Meimoun P, Errakhi R, Madiona K, Barakate M, Bouteau F (2008). Toxic and signalling effects of oxalic acid: Oxalic acid-Natural born killer or natural born protector? Plant Signal. Behav. 3:746-748.

Li Y, Wang Y, Jiang H, Deng J (2009). Crystal structure of Manduca sexta prophenoloxidase provides insights into the mechanism of type 3 copper enzymes. Proc. Natl. Acad. Sci. USA 106:17002-17006.

Lü ZR, Shi L, Wang J, Park D, Bhak J, Yang JM, Park YD, Zhou HW, Zou F (2010). The effect of trifluoroethanol on tyrosinase activity and conformation: inhibition kinetics and computational simulations. Appl. Biochem. Biotechnol. 160:1896-1908.

Morris GM, Huey R, Lindstrom W, Sanner MF, Belew RK, Goodsell DS, Olson AJ (2009). AutoDock4 and AutoDockTools4: Automated docking with selective receptor flexibility. J. Comput. Chem. 30, 2785-2791.

Nakata PA, He C (2010). Oxalic acid biosynthesis is encoded by an operon in Burkholderia glumae. FEMS Microbiol. Lett. 304:177-182.

Olivares C, Solano F (2009). New insights into the active site structure and catalytic mechanism of tyrosinase and its related proteins. Pigment Cell Melanoma Res. 22:750-760.

Park YD, Kim SY, Lyou YJ, Lee JY, Yang JM (2005). A new type of uncompetitive inhibition of tyrosinase induced by Cl^- binding. Biochimie 87:931-937.

Park YD, Kim SY, Lyou YJ, Lee DY, Yang JM (2006). TXM13 human melanoma cells: a novel source for the inhibition kinetics of human tyrosinase and for screening whitening agents. Biochem. Cell Biol. 84:112-116.

Park YD, Lyou YJ, Hahn HS, Hahn MJ, Yang JM (2006). Complex inhibition of tyrosinase by thiol-composed Cu^{2+} chelators: a clue for designing whitening agents. J. Biomol. Struct. Dyn. 24:131-138.

Rescigno A, Sollai F, Pisu B, Rinaldi A, Sanjust E (2002). Tyrosinase inhibition: general and applied aspects. J. Enzyme Inhib. Med. Chem. 17:207-218.

Sayyari M, Valero D, Babalar M, Kalantari S, Zapata PJ, Serrano M (2010). Prestorage oxalic acid treatment maintained visual quality, bioactive compounds, and antioxidant potential of pomegranate after long-term storage at 2 degrees C. J. Agric. Food Chem. 58:6804-6808.

Shiino M, Watanabe Y, Umezawa K (2001). Synthesis of N-substituted N-nitrosohydroxylamines as inhibitors of mushroom tyrosinase. Bioorg. Med. Chem. 9:1233-1240.

Shiino M, Watanabe Y, Umezawa K (2003). Synthesis and tyrosinase inhibitory activity of novel N-hydroxybenzyl-N-nitrosohydroxylamines. Bioorg. Chem. 31:129-135.

Xie MX, Xu XY, Wang YD (2005). Interaction between hesperetin and human serum albumin revealed by spectroscopic methods. Biochim. Biophys. Acta 1724:215-224.

Yamazaki Y, Kawano Y, Yamanaka A, Maruyama S (2009). N-[(Dihydroxyphenyl)acyl]serotonins as potent inhibitors of tyrosinase from mouse and human melanoma cells. Bioorg. Med. Chem. Lett. 19:4178-4182.

Yan Q, Cao R, Yi W, Yu L, Chen Z, Ma L, Song H (2009). Synthesis and evaluation of 5-benzylidene(thio)barbiturate-beta-D-glycosides as mushroom tyrosinase inhibitors. Bioorg. Med. Chem. Lett. 19:4055-4058.

Yokota T, Nishio H, Kubota Y, Mizoguchi M (1998). The inhibitory effect of glabridin from licorice extracts on melanogenesis and inflammation. Pigment Cell Res. 11:355-361.

Yoon J, Fujii S, Solomon EI (2009). Geometric and electronic structure differences between the type 3 copper sites of the multicopper oxidases and hemocyanin/tyrosinase. Proc. Natl. Acad. Sci. USA 106:6585-6590.

Zoppi A, Lofrumento C, Mendes NF, Castellucci EM (2010). Metal oxalates in paints: a Raman investigation on the relative reactivities of different pigments to oxalic acid solutions. Anal. Bioanal. Chem. 397:841-849.

Zou QJ, Liu SY, Dong XY, Bi YH, Cao YC, Xu Q, Zhao YD, Chen H (2007). In vivo measurements of changes in pH triggered by oxalic acid in leaf tissue of transgenic oilseed rape. Phytochem. Anal. 18, 341-346.